


ARTICLE

Open Access



Inhibitory potential of rutin and rutin nano-crystals against *Helicobacter pylori*, colon cancer, hemolysis and Butyrylcholinesterase in vitro and in silico

Husam Qanash^{1,6}, Aisha M. H. Al-Rajhi^{2*}, Majed N. Almashjary^{3,4}, Ammar A. Basabrain^{3,4},
Mohannad S. Hazzazi^{3,4} and Tarek M. Abdelghany^{5*} 

Abstract

Despite the vital activity of many compounds, they lack that effectiveness due to their low solubility in water. Unfortunately, for this reason, rutin often leads to low tissue permeability and insufficient bioavailability, which has greatly limited its pharmacological utility. Therefore, the present investigation is designed to overcome this problem by formulating the rutin to rutin nanocrystals (RNCs) with studying their some pharmacological applications in vitro and in silico. RNCs were created via the ultrasonication approach and showed a spherical shape via Transmission electron microscopy with a mean particle size of 27 nm. RNCs reflected inhibitory action against *Helicobacter pylori* with an inhibition zone (IZ) of 22.67 mm compared to rutin (IZ of 18 mm) and standard control (IZ of 19.5 mm). RNCs exhibited less minimum inhibitory concentration (MIC) and minimum bactericidal concentration (MBC) (7.8 µg/mL) than rutin (62.5 µg/mL). The MBC/MIC index of rutin and RNCs indicated their bactericidal properties. RNCs were more acutely (92.12%) than rutin (85.43%) for inhibition the *H. pylori* biofilm formation. A promising half maximal inhibitory concentration (IC₅₀) (6.85 µg/mL) was recorded using RNCs for urease inhibition compared to the IC₅₀ value of rutin (97.8 µg/mL). The activity of rutin and RNCs was tested against cancer cells of human colon cancer (HT-29) and normal Vero cells. IC₅₀ values of RNCs were less 168.23 ± 1.15 µg/mL and 297.69 ± 4.23 µg/mL than the IC₅₀ values of rutin 184.96 ± 4.33 µg/mL and 335.31 ± 2.02 µg/mL against HT-29 cells and normal Vero cells, respectively. Different percentages (72.2, 77.3, and 81.9%) of hemolysis inhibition were recorded using RNCs, but 63.6, 68.9, 73.6, and 80.6% were obtained using rutin at 600, 800, and 1000 µg/mL, respectively. Butyrylcholinesterase (BChE) inhibition % was documented at a lower IC₅₀ value for RNCs (12.74 µg/mL) than the IC₅₀ of rutin (18.15 µg/mL). The target molecule underwent molecular docking research against *H. pylori* [Protein Data Bank (PDB) code: 4HI0], HT-29 cells (PDB code: 2HQ6), and BChE (PDB code: 6EMI) in order to enhance the interactions between rutin and the chosen receptors and to estimate its molecular operating environment (MOE) affinity scoring. Rutin has predicted strong binding interactions and potent activity against the examined proteins 4HI0, 2HQ6, and 6EMI with low binding scores of - 7.47778 kcal/mol, - 7.68511 kcal/mol, and - 9.50333 kcal/mol, respectively.

Keywords Rutin, Nanocrystals, *Helicobacter pylori*, Butyrylcholinesterase, Molecular docking, Hemolysis

*Correspondence:

Aisha M. H. Al-Rajhi
amoalrajhi@pnu.edu.sa

Tarek M. Abdelghany
tabdelghany.201@azhar.edu.eg

Full list of author information is available at the end of the article



© The Author(s) 2023. **Open Access** This article is licensed under a Creative Commons Attribution 4.0 International License, which permits use, sharing, adaptation, distribution and reproduction in any medium or format, as long as you give appropriate credit to the original author(s) and the source, provide a link to the Creative Commons licence, and indicate if changes were made. The images or other third party material in this article are included in the article's Creative Commons licence, unless indicated otherwise in a credit line to the material. If material is not included in the article's Creative Commons licence and your intended use is not permitted by statutory regulation or exceeds the permitted use, you will need to obtain permission directly from the copyright holder. To view a copy of this licence, visit <http://creativecommons.org/licenses/by/4.0/>.

Introduction

Well-known natural compounds are currently helpful in biomedicine because of their high levels of safety, economic viability, and biological impacts. Rutin is a natural polyphenolic flavonoid compound, also referred to as vitamin P, with an intriguingly broad medicinal range. Chemically, rutin is referred as quercetin-3-rutinoside or 2-(3,4-dihydroxyphenyl)-4,5-dihydroxy-3-[3,4,5-trihydroxy-6-[(3,4,5-trihydroxy-6-methyl-oxan-2-yl)oxymethyl]oxan-2-yl]oxy-chromen-7-one. According to Mauludin et al. [1], it was discovered in several plants, such as buckwheat, green tea, and citrus fruits, including grapefruit, orange, lemon, and lime, besides apples.

The vast range of pharmacological activities, natural sources, safety, and cost-effectiveness of rutin make it an appealing medicine [2]. Additionally, numerous studies [3–5] have demonstrated that rutin has antioxidant, antidiabetic, anticancer, anti-inflammatory, antibacterial, anti-arthritic, and neuroprotective effects. The antihypertensive, cardioprotective, antispasmodic, anti-thrombotic, and anti-hyperlipidemia effects of rutin have also been validated [6, 7]. According to research by Orhan et al. [8], rutin has been proven to have potent antibacterial and antifungal effects against human and food-borne pathogens, including *Staphylococcus aureus*, *Acinetobacter baumannii*, *Pseudomonas aeruginosa*, and *Candida krusei*. Rutin has some disadvantages, including poor water solubility, poor bioavailability, constricted stability, and restricted membrane permeability, despite its intriguing pharmacological, therapeutic, and nutritional benefits [9].

Numerous formulation techniques and drug delivery methods have been used to increase rutin's therapeutic effectiveness and overcome these drawbacks. Dried rutin nanocrystals (RNCs), for instance, have been produced and added to tablets [1]. Nanocrystals (NCs) are sub-micron colloidal dispersions that are entirely made up of drug substances. They were initially launched in the 1990s as a way to enhance the aqueous solubility and bioavailability of medicines with low water solubility [5]. NCs are commonly created by grinding bulk drug material and have a particle size in the nanometer range [10]. Surfactants, polymers, or both stabilize NCs in various ways. The tablets of NCs achieved 100 % rutin dissolution in 30 min compared to microcrystal and commercialized tablets, which achieved only 71% and 55% dissolution, respectively. Rutin-loaded silver nanoparticles were fabricated, and their anti-thrombotic activity was evaluated [11]. In a recent report, the dissolution rate and drug aqueous solubility were increased 2.3- to 6.7-fold and 102- to 202-fold as a result of the formulation of rutin into RNCs [5]. Rutin's improved water solubility and effectiveness compared to traditional administration

were validated by the creation of RNCs for the various therapeutic objectives [3]. Positively charged nanoparticles are more effective than negatively charged ones at enhancing the absorption profile. Rutin in NCs construction is more efficient for various therapeutic activities via aqueous solubility enhancement compared to rutin in non-NCs form [3]. When compared to bulk rutin, RNCs minimum inhibitory concentration (MIC), biofilm, and adhesion inhibitory properties were studied for several bacterial species. It was discovered that the aqueous dispersion of RNCs was significantly more efficient than the conventional delivery of rutin against *Pseudomonas aeruginosa*, *Staphylococcus aureus*, *Escherichia coli*, *Enterococcus faecalis*, *Streptococcus mutans*, *Klebsiella pneumoniae*, and *Acinetobacter baumannii* [4].

The most common type of neurological disorder is Alzheimer's disease, which is characterized by persistent memory loss, cognitive dysfunctions, and behavioral imbalances. Several drugs are now used to treat Alzheimer's disease, but they each have a unique set of side effects on health. Scientists have been concentrating on plants as an alternate method of treating or managing Alzheimer's disease as well as other diseases [12–14]. In an in vivo study, Xu et al. [15] demonstrated that rutin via oral administration attenuated memory deficits in Alzheimer's illness transgenic mice, reduced levels of oligomeric β -amyloid, glutathione disulfide, and malondialdehyde levels, as well as increased activity of superoxide dismutase in the brain. Habtemariam [16] mentioned that rutin can control the cognitive as well as several behavioral symptoms of Alzheimer's disease due to its capability to cross the blood-brain barrier. Rutin is one of the flavonoids with the most extensive applications as an antioxidant and an antitumor agent among flavonoids due to its abundance in foods like fruits and vegetables that are consumed by people [17]. The effect of rutin on cancer cell line proliferation, like breast, prostate, colon, and lung, was investigated in numerous studies in vitro as mentioned in the review study by Satari et al. [18].

In silico approaches are promising scientific tools for studying and understanding the mechanisms of biological processes. One of the in silico approaches is molecular docking, which is used to investigate the appropriateness of any drug before its application [19–23]. Currently, computer-aided drug designing mainly depends on the molecular docking approach for the identification of new pharmacological agents. Also, molecular docking approaches play a critical role in discovering and developing of drugs by studying the interaction a drug receptor or predicting the activity and affinity of a ligand to the binding site of target cell proteins. However, rutin was experimented on the management of several illnesses but its NCs do not cover most of the studied illnesses. So the

current investigation aimed to preparation of RNCs and their evaluation against *H. pylori* growth, cancer proliferation, hemolysis, and butyrylcholinesterase as a marker of Alzheimer's disease development. Also, the molecular docking interactions of the rutin with *H. pylori*, cancer cells, and butyrylcholinesterase were assigned.

Materials and methods

Source of used chemicals, normal, cancer cell lines and tested *H. pylori*

Rutin (RT) (purity > 95%) and Tween 80 were purchased from Sigma-Aldrich (St. Louis, MO, USA). Other used chemicals including reagents, solvents, and microbial growth media were obtained from El-Gomhouria Company and United Company for Chemicals and Medical Preparations, Cairo, Egypt. American Type Culture Collection (ATCC) was the source of normal and cancer cell lines. Ain Shams University Hospitals; Cairo Egypt was the source of *H. pylori*.

Creation of rutin nanocrystals and their characterization

An ultrasonication approach was applied to prepare rutin nanocrystals (RNCs). A mixture of ethanol and hexane was used as a solvent (25/75 v/v) of rutin (50 mg/mL). The reaction mixture was subjected to ultrasonication at a frequency of 50 kHz using an ultrasonic source. Then, 2% of tween 80 (a surfactant) was added as a surfactant to the mixture. The mixture was centrifuged for 30 min at 1000 rpm. Via rotary evaporation, the resulting solution was evaporated while the obtained precipitate yellow powder was used as rutin nanoparticles [5]. The size and shape of rutin and RNCs were photographed by Transmission electron microscopy (TEM), model JEOL 1010 manufactured in Japan. The rutin and RNCs were dropped on a carbon-coated copper-grid, and then inserted in a specimen holder. Fourier Transform Infrared Spectroscopy (FTIR) (Shimadzu 8400S, Japan) was applied to identify the FTIR spectra of the rutin and RNCs via mixing and compressing these compounds with the potassium bromide (FTIR grade).

Anti-*H. pylori* activity, MIC and MBC of rutin and RNCs

The well diffusion technique was utilized to assess the Anti-*H. pylori* activity of rutin and RNCs. In the beginning, the colonies of *H. pylori* were put in McFarland's 0.5 Muller Hinton fluid. Subsequently, *H. pylori* was cultivated on supplemented Muller Hinton agar with 5% horse blood. The diameter of the inhibition zone around the well was measured after 5 days of incubation at 37 °C and under microaerophilic conditions. Clarithromycin was used as a positive control [24].

The minimum inhibitory concentration (MIC) and minimum bactericidal concentration (MBC) of rutin and RNCs were detected against *H. pylori*. In 96-flat well microplates, the rutin and RNCs underwent the MTT tetrazolium reduction evaluation. At different quantities ranging from 7.8 to 500 g/mL, the rutin and RNCs were dissolved in Brucella broth. The plate wells were filled with 50 µL of 2×10^5 cells/mL of *H. pylori*, and then incubated. The MTT reduction experiment was used to determine the MIC, which is the smallest concentration of rutin and RNCs in the plate at which no *H. pylori* growth occurred. We added 15 L of MTT to the rutin and RNCs before incubating them for 15 min, after which the formazan crystals were dissolved by the addition of 80 µL of DMSO. At 570 nm, the absorbance was recorded in the microplate readers (DTX 800/880 Multimode Detectors, Fullerton, CA) to detect the MIC. MBC was detected by mixing 50 µL aliquots of preparations that showed no *H. pylori* growth after the incubation period during the MIC test with 150 µL of sufficient broth [25]. These preparations were incubated at 37 °C for 72 h under microaerophilic conditions. MBC was assumed to have the lowest concentration of rutin or RNCs which did not develop any color change after MTT addition as described above.

Anti-biofilm activity of rutin and RNCs

In 96-well polystyrene flatbottom plates, the impact of rutin and RNCs on the development of *H. pylori* biofilms was assessed. Trypticase soy yeast broth (TSY) (300 µL) was inoculated with 10^6 CFU/mL of *H. pylori*, and then transferred to wells of a microplate with the existence of the previously established sub-lethal quantities of MBC (75, 50, and 25%). As controls, wells containing medium with methanol and without rutin or RNCs were employed. For 48 h, plates were incubated at 37 °C. After the incubation period, the supernatant was removed, and each well was carefully washed with sterile distilled water to eliminate free-floating cells. The plates were then allowed to air dry for 30 min, and the biofilm that had developed was stained for 15 min at room temperature with a 0.1% crystal violet aqueous solution.

After incubation, the excess of crystal violet was removed by washing the plates three times with sterile distilled water. Finally, 250 µL of 95% ethanol was added to each well to solubilize the cell-bound dye, incubated for 15 min, and then measured for absorbance at a wavelength of 570 nm using a microplate reader [26]. *H. pylori* biofilm inhibition was calculated according to the subsequent formula:

$$\text{Biofilm inhibition} = 1 - \left(\frac{\text{Absorbance at treatment} - \text{Absorbance at blank}}{\text{Absorbance at control} - \text{Absorbance at blank}} \right) \times 100$$

Assay of urease activity

With some modification on the Berthelot spectrophotometric approach, urease inhibition by rutin and RNCs was assayed at 625 nm [27]. The reaction mixture contained 850 μL of urea and different concentrations of rutin and RNCs ranged from 1.95 to 1000 $\mu\text{g}/\text{mL}$ with 100 mM phosphate buffer (pH 7.4). To start the enzymatic reaction, 15 μL of urease enzyme was added to the reaction mixture. Then after 1 h, the concentration of liberated ammonia was measured utilizing 1000 μL of solutions A and B (500/500 v/v). Solution A was prepared from 2.5 mg of sodium nitroprusside and 0.5 g phenol dissolved in 50 mL of H_2O , while solution B was prepared from 250 mg of NaOH and 820 μL of NaOCl 5% dissolved in 50 mL of H_2O at the temperature of 37 $^\circ\text{C}$ for 30 min. Uninhibited urease activity was selected as 100% of the control activity. The enzymatic reaction value was calculated from the following formula:

$$\text{Urease inhibition\%} = 1 - \left(\frac{\text{AbT}}{\text{AbC}} \right) \times 100$$

where AbT is the absorbance of the tested rutin or RNCs or positive control in the existence of urease, AbC is the absorbance of the solvent in the existence of urease. The activity of tested samples was compared to the standard compound hydroxyurea which is already shown to have inhibitory action for urease enzyme. The concentration that stimulates the inhibition halfway among the minimum and maximum response of rutin or RNCs (IC_{50}) was determined by observing the inhibition influence of different concentrations of tested samples in the examination. The values of IC_{50} were assayed utilizing Graph-Pad Prism 5 software.

Butyrylcholinesterase activity assay

BChE hydrolysis of S-butrylthiocholine iodide (BTC) (0.05–0.4 mM) was recorded spectrophotometrically in MOPS buffer (50 mM, pH 8) at 25 $^\circ\text{C}$ in the existence of 5,5'-dithiobis(2-nitrobenzoic acid) (DTNB) (0.125 mM) based to the Ellman method. The reactions were started by adding 0.2 U/mL BChE. The rate of increase of absorbance was monitored at 405 nm on a Biosystem – 310 spectrophotometer. The activity of BChE was assessed based on the linear segments of the progress curves in the initial 60 sec period utilizing the extinction coefficient of 14.2 $\text{mM}^{-1}/\text{cm}^{-1}$. BChE inhibition was planned by adding 0–0.375 μM DMMB to the reaction mixture (final volume was 1.2 mL). Enzyme activity was not affected by the existence of methanol ($\leq 1.25\%$, v/v) in the reaction mixture [28, 29].

Cytotoxicity detection of Rutin and RNCs using MTT assay

Two types of cells were used to measure the cytotoxicity of rutin and RNCs including normal Vero cells (Organism: *Cercopithecus aethiops*, Tissue: Kidney, Cell type: Epithelial, Culture properties: Adherent, Disease: Normal, ATCC: CCL-81) and human colon cancer (HT-29) (Organism: *Homo sapiens* Human, Tissue: Colon, Cell type: Epithelial, Culture properties: Adherent, Disease: Adenocarcinoma Colorectal, ATCC: HTB-38). Rutin and RNCs were dissolved in dimethyl sulfoxide. The 96-well tissue culture plate was injected with 1×10^5 tested cells per mL (100 μL per well), and then let to establish a full monolayer sheet for 24 h at 37 $^\circ\text{C}$. Subsequently, a confluent cells sheet had grown, the 96 well micro-titer plates' growth material was decanted, and the cell monolayer was double washed using wash media. The rutin or RNCs were diluted twice in RPMI medium containing 2% of serum. In examine wells; 0.1 mL of each dilution was examined, leaving 3 wells as controls that just received RPMI medium. The plate was examined after 37 $^\circ\text{C}$ of the incubation period to check any signs of toxicity on the tested cells. Each well was amended with 20 μL of the prepared MTT solution (5 mg/mL in PBS), followed by shaking for 5 min at 150 rpm to mix the MTT into the RPMI medium. The plate containing wells was incubated for 4 h under certain conditions of CO_2 (5%) and 37 $^\circ\text{C}$ to permit the MTT to be metabolized. The plate was dried using paper towels to remove any residue from the media. Using 200 μL of DMSO, the formazan (MTT metabolic product) was resuspended via shaking for 5 min at 150 rpm to allow the mixing of the formazan into the DMSO [12]. The optical density was measured at 570 nm. The viability of cells was calculated using the subsequent formula:

$$\text{Cell Viability(\%)} = \frac{\text{Absorbance at treatment cells}}{\text{Absorbance at untreated cells}} \times 100$$

An inverted light microscope (Leica Microsystems, Leica DM IL LED, Germany) was used to image the morphological changes in the incubated cells.

Preparation of erythrocyte suspension for hemolysis inhibition

Healthy participants' fresh whole blood (3 mL) was drawn into heparinized tubes and centrifuged for 10 min at 3000 rpm. The red blood pellets were dissolved in a volume of normal saline that was equal to the volume of the supernatant. A 40% v/v suspension of the acquired dissolved red blood pellets was made using an isotonic buffer solution (10 mM sodium phosphate buffer, pH 7.4) after the volume of the pellets was determined. In one L of distilled H_2O , the buffer solution included 0.2 g of

NaH_2PO_4 , 1.15 g of Na_2HPO_4 , and 9 g of NaCl. Red blood cells that had been reconstituted (resuspended supernatant) were applied in this way.

In distilled water, rutin or RNCs were dissolved (hypotonic solution). The centrifuge tubes were filled with duplicate pairs (per dosage) of the hypotonic solution (5 mL) containing graded doses of the investigated substance (100, 200, 400, 600, 800, and 1000 $\mu\text{g}/\text{mL}$). Additionally, duplicate pairs (per dosage) of centrifuge tubes were filled with an isotonic solution (5 mL) containing graded doses of the extracts (100–1000 $\mu\text{g}/\text{mL}$). 5 mL of the vehicle (distilled water) and 5 mL of indomethacin 200 $\mu\text{g}/\text{mL}$ were each included in the control tubes. Each tube received 0.1 mL of erythrocyte suspension, which was gently mixed in. The mixtures were then centrifuged for 3 min. at 1300g after being incubated for 1 h. at room temperature (37 °C). Using a Spectronic (Milton Roy) spectrophotometer, the haemoglobin concentration of the supernatant's absorbance (OD) was calculated at 540 nm. By assuming that all hemolysis generated in the presence of distilled water is 100%, the percentage of hemolysis was estimated [21]. The extract's inhibition of hemolysis (%) was determined as follows:

$$\text{Haemolysis inhibition(\%)} = 1 - \left(\frac{\text{OD}_2 - \text{OD}_1}{\text{OD}_3 - \text{OD}_1} \right) \times 100$$

where OD1 = absorbance of rutin or RNCs in isotonic solution, OD2 = absorbance of rutin or RNCs in hypotonic solution, OD3 = absorbance of control sample in hypotonic solution.

Molecular docking experiment of rutin

A molecular operating environment (MOE) is an amalgamation of software programs used to create biologically active compounds or a package. It allows for the possibility to drawing molecules and minimizing them for optimal conformations. Rutin structure was drawn using ChemDraw Ultra 15.0, and this structure was saved as MDL files (".sdf") for MOE2019 to show. The Crystal Structure of *H. pylori* [(Protein Data Bank (PDB) code: 4HI0), Colon cancer (PDB code: 2HQ6), and Butyrylcholinesterase (PDB code: 6EMI) have been downloaded from the protein data bank (<https://www.rcsb.org/> accessed on 10 April 2021). After the water molecules and co-ligand were extracted, the protein molecule undergoes 3D protonation. The protein was exhibited using the MMFF94x force field implemented in the MOE 2019 software. While the side chains are still flexible, the main chain has been kept rigid. The side chains of the proteins can locate the location where interactions are most favorable attributable to this approximation. The lowest energy result correlates to the best interactions between the ligand and the enzyme's active site, thus we

then logged that result as the best score (S, kcal/mol). The MOE program's dock scoring was calculated using the London dG scoring formula, placement: triangle matcher, retain 10, and refinement: force field. The leading conformations of the docked ligands were determined by taking into account the Root Mean Square Deviation (RMSD) values, binding energies, and binding modes with the chosen residues.

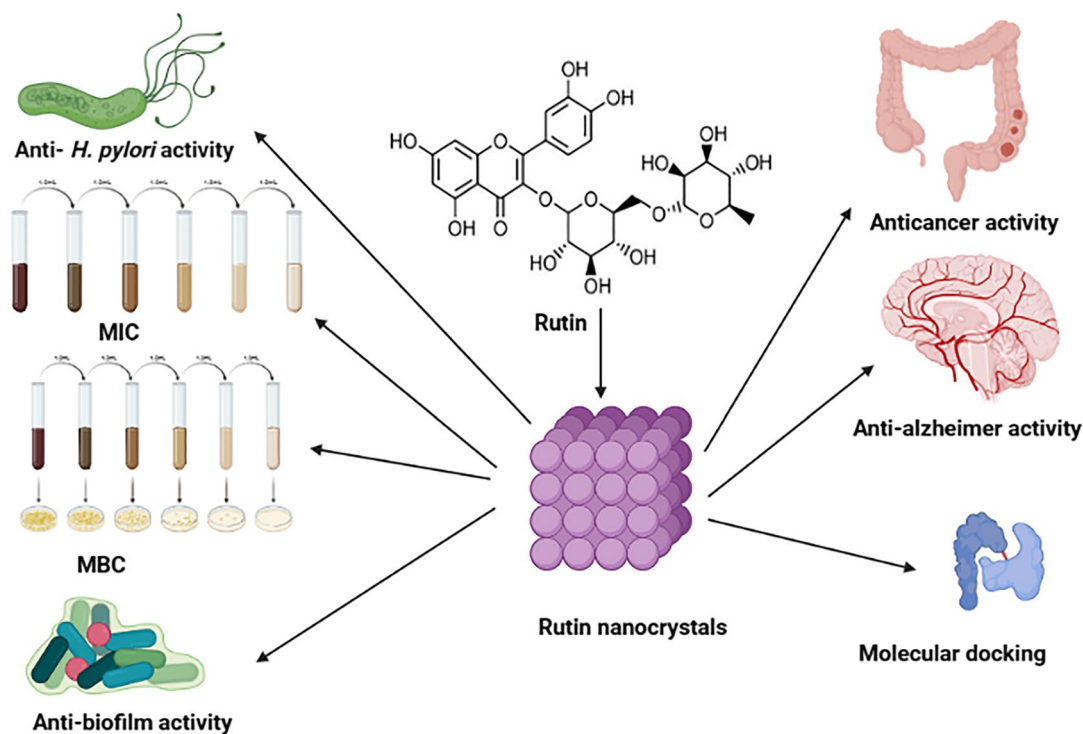
Statistical analysis

Outcomes are detected as mean \pm SD (standard deviation) and the results were taken three times. Statistical program of computer programs Microsoft Excel version 365 and SPSS v.25 (statistical package for the social science version 25.00) were applied to calculate statistical analysis. Quantitative data with parametric distribution between the various treatments were done using variance analysis for the one-way ANOVA and Post hoc-Tukey's test, at 0.05 probability levels.

Results and discussion

Prepared RNCs and characterization

Unfortunately, certain chemicals' extremely low water solubility frequently results in their poor permeability into cells and tissues as well as inadequate bioavailability, which has severely constrained their use in pharmacology. One of these compounds is rutin (Empirical formula $\text{C}_{27}\text{H}_{30}\text{O}_{16}$), therefore nano-formulation was developed to overcome this problem. In the present study, rutin was transformed into rutin nanocrystals (RNCs) via the ultrasonication process, and then some pharmacological applications were evaluated as summarized in Fig. 1. TEM showed that the mean particle size of the prepared RNCs was 27 nm with the spherical shape of the most detected RNCs. On the other hand, rutin appeared in bulk mass that not differentiated into RNCs (Fig. 2). Bohlouli et al. [30] found that the created RNCs exhibited a mean size of 75 nm using the same method of synthesis. The differences in RNCs size may be due to the potency of the sonication process. Slight differences were observed between FTIR analysis of rutin and RNCs indicating that the chemical composition of rutin was not affected during the sonication process. Our results were in agreement with other findings [4, 30]. More than 20 similar bands were detected in the FTIR analysis of rutin and RNCs, for instance, the detected bands 3423.36, 1656.52, 1599.71, 1572.91, 1555.98, 1504.85, 1456.94, 1362.06, 1294.85, 1234.25, 1203.67, 1012.16, 969.85, 878.94, 806.41, 688.55, 726.17, 655.42, 630.15, 595.90, and 531.59 cm^{-1} in rutin were similar to the detected bands 3423.23, 1655.58, 1598.82, 1573.57, 1556.63, 1504.97, 1457.86, 1361.17, 1295.60, 1236.47, 1204.21, 1012.83, 970.90, 878.98, 806.51, 687.89, 725.93, 655.47, 630.60,



Created in BioRender.com

Fig. 1 Rutin transformed to RNCs and their performed activities including Anti-*H. pylori* activity, Minimum inhibitory concentration (MIC), Minimum bacteriocidal concentration (MBC), anticancer activity, anti-Alzheimer activity, and molecular docking

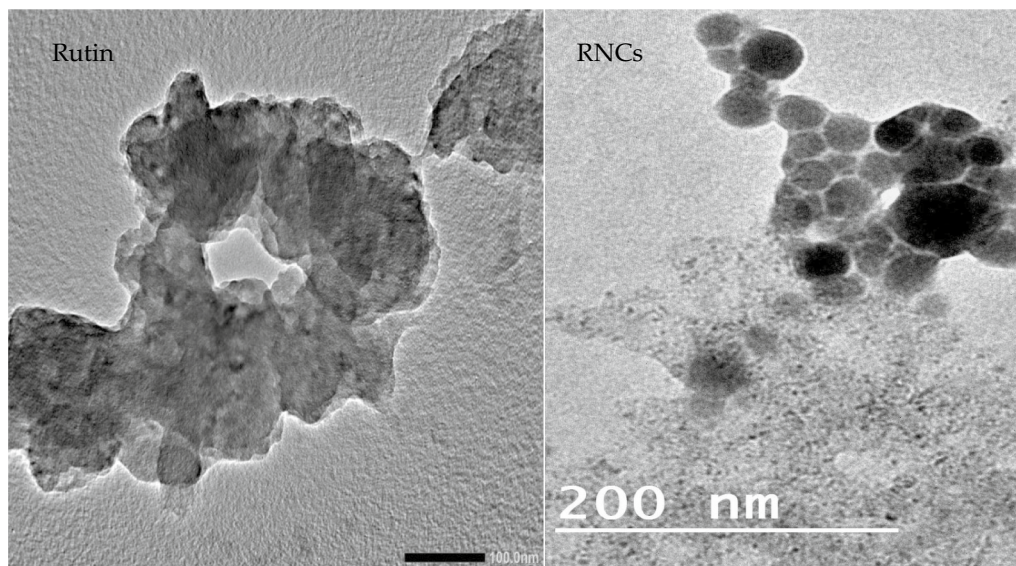


Fig. 2 TEM of rutin and RNCs which reflected particle size 27 nm of RNCs with spherical while rutin appeared in bulk mass

596.19, and 531.76 cm^{-1} in RNCs. The detected peaks at 3423 cm^{-1} , 1456.94 cm^{-1} , and 1736 cm^{-1} are associated with the OH, ketone, and ester groups, respectively

(Additional file 1). The similarity of most detected bands in rutin and RNCs analysis by FTIR indicating that ultrasonication process did not affect the rutin structure.

Anti-*H. pylori* activity of rutin and RNCs

RNCs exhibited anti-*H. pylori* activity with a significantly ($p < 0.05$) inhibition zone of 22.67 mm while rutin exhibited less inhibition zone of 18 mm (Fig. 3 and Table 1). At the same time, the activity of rutin and RNCs compared to the positive control (Clarithromycin) gave an inhibition zone of 19.5 mm. MIC and MBC of RNCs (7.8 $\mu\text{g}/\text{mL}$) were less than MIC and MBC of rutin (62.5 $\mu\text{g}/\text{mL}$). The obtained values of MBC/MIC index indicated the bactericidal properties of rutin and RNCs as well as positive control. Rutin activity against *H. pylori* is described previously [31]. The probable mechanisms of nano-drugs interaction with microbial cells, they may fuse with microbial cells surface leading to enhancing the drug's permeability into the cells; or they are absorbed on the cell wall and operate as a depot to discharge active drug [32]. In the biofilm formation of *H. pylori* was more affected by RNCs compared to rutin at all used doses of MBC, where at 25 %, 50 % and 75 % of MBC, the anti-biofilm % was 64.59, 71.52 and 85.43 % using rutin, while it was 70.74, 84.02 and 92.12 % using RNCs, respectively (Fig. 4A), which documented also by a color change of stained *H. pylori* biofilm in the microtiter plate (Fig. 4B). Exopolysaccharides play an important role in bacterial biofilms to resist antimicrobial drugs. Biofilm formation of *S. aureus* and *E. coli* was inhibited as a result of

exposure to rutin [33] via reduction of exopolysaccharides production. According to Wang et al. [34] rutin exhibited strong inhibition against growth and biofilm formation of *E. coli* and *K. pneumoniae* with MIC 512 $\mu\text{g}/\text{mL}$ and 1024 $\mu\text{g}/\text{mL}$, respectively. The inhibitor potential of rutin and RNCs against *H. pylori* was documented via the detection of urease activity. Urease inhibition increased with the increment of rutin and RNCs concentrations in the range of 1.95 to 1000 $\mu\text{g}/\text{mL}$, but the highest inhibitory action was observed using RNCs compared to rutin at all applied concentrations. For instance, at 1.95, 7.18, and 250 $\mu\text{g}/\text{mL}$, the urease inhibition was 35, 43.5 and 82.3% using RNCs compared to the 8.4, 22.9 and 59.1% of urease inhibition, respectively caused by rutin (Fig. 5). Promising IC_{50} (6.85 $\mu\text{g}/\text{mL}$) was recorded for urease inhibition using RNCs while rutin exhibited IC_{50} value of 97.8 $\mu\text{g}/\text{mL}$.

Cytotoxic activity of rutin and RNCs was performed against the proliferation of HT-29 cells and normal Vero cells (Fig. 6). Cytotoxicity against HT-29 cells increased with the increment concentrations of rutin and RNCs up to 1000 $\mu\text{g}/\text{mL}$. At a low concentration of 31.25 $\mu\text{g}/\text{mL}$, RNCs exhibited no toxicity against HT-29 while rutin exhibited very low toxicity (0.23 %). A remarkable effect on the HT-29 cells was observed at concentrations 62.5 to 1000 $\mu\text{g}/\text{mL}$ of rutin and RNCs where

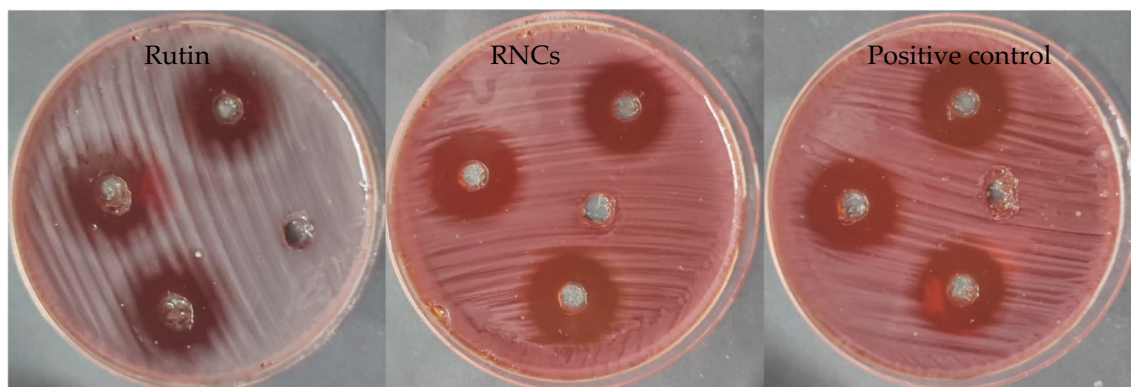


Fig. 3 Anti-*H. pylori* activity of rutin, RNCs and positive control (Clarithromycin) (Three wells with inhibition zone) using Muller Hinton agar with 5% horse blood. Well without inhibition zone in each plate indicating the negative control (Solvent)

Table 1 Inhibitor activity, MIC and MBC of rutin and RNCs against *H. pylori*

Treatment	Inhibitions zones mean (mm)	MIC ($\mu\text{g}/\text{mL}$)	MBC ($\mu\text{g}/\text{mL}$)	MBC/MIC index
Rutin	18.00 \pm 0.00	62.5	62.5	1.0
RNCs	22.67 \pm 0.58	7.8	7.8	1.0
Positive control (Clarithromycin)	19.5 \pm 0.50	31.25	31.25	1.0
Negative control (Solvent)	0.0 \pm 0.0	0.0	0.0	0.0

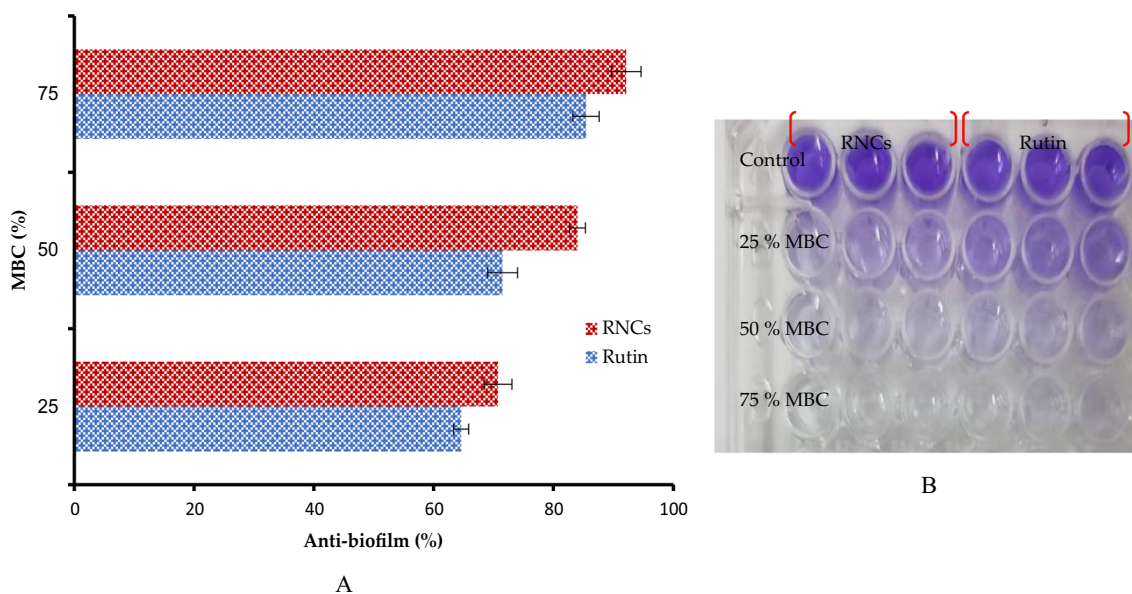


Fig. 4 Effect of different MBC (%) of rutin and RNCs against biofilm formation of *H. pylori* (A), Microtiter plate revealed stain color alterations as an pointer of increased anti-biofilm formation (B) at various treatments including Media + *H. pylori* (Control); 25% of MBC; C 50% of MBC, and 75% of MBC

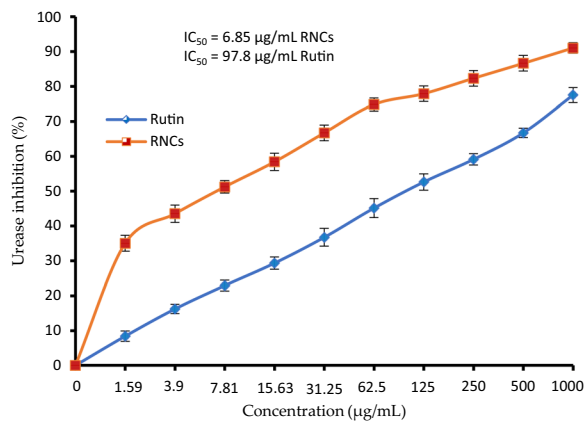


Fig. 5 Urease inhibition (%) of *H. pylori* at different concentrations of rutin and RNCs up to 1000 µg/mL with IC₅₀ values

the toxicity was 97.01 and 97.06 %, respectively. RNCs reflected significantly high cytotoxicity (40.11 and 80.45 %) ($p < 0.05$) at 125 µg/mL and 250 µg/mL, respectively, compared to the cytotoxicity (24.12 and 77.29 %) of rutin at the same concentrations. The IC₅₀ value of RNCs was less (168.23 ± 1.15 µg/mL) than the IC₅₀ value 184.96 ± 4.33 µg/mL of rutin against HT-29 cells

Up to 125 µg/mL, rutin and RNCs showed a negligible cytotoxic effect, against normal Vero cells at level less than 1% (Fig. 6), while at 250 to 1000 µg/mL, these compounds reflected toxicity. Unfortunately, the IC₅₀ value

of RNCs was less (297.69 ± 4.23 µg/mL) than the IC₅₀ value of rutin (335.31 ± 2.02 µg/mL) against Vero normal cells. However, from the obtained IC₅₀ values of rutin and RNCs against HT-29 and Vero normal cells, the application of RNCs at their IC₅₀ values may affect cancer cells but not normal cells. Nanoemulsion of rutin reflected strong anticancer potential against prostate carcinoma cells compared to bulk rutin [35]. Also, Asfour and Mohsen [36] enhanced the anticancer potential of rutin via rutin nanospheres development. Viability reduction of HT-29 colon cancer cells was recorded using rutin that stimulated the apoptotic cycle depending on mitochondria by controlling the Bax and Bcl-2 expression, accelerating the cleaved caspases-3, -8 and -9 [37]. The findings of Bohlouli et al. [30] showed no cytotoxic effect of rutin on HN5 cells up to 2000 µM, while RNCs exhibited a decline in viability of the cells in a concentration- and time-dependent manner with IC₅₀ values of 30.51 µM and 27.34 µM at 1 and 2 days of incubation period, respectively. According to Bohlouli et al. [30], RNCs reflected anticancer activity at least 100 times compared to bulk rutin.

Image analysis using the inverted microscope reflected the morphological changes of HT-29 and Vero normal cells exposed to the different concentrations of rutin and RNCs. At low concentrations (31.25 µg/mL and 62.5 µg/mL) of rutin, there are no appeared morphological changes in HT-29, while at 250 to 1000 µg/mL remarkable changes were recorded particularly at 500

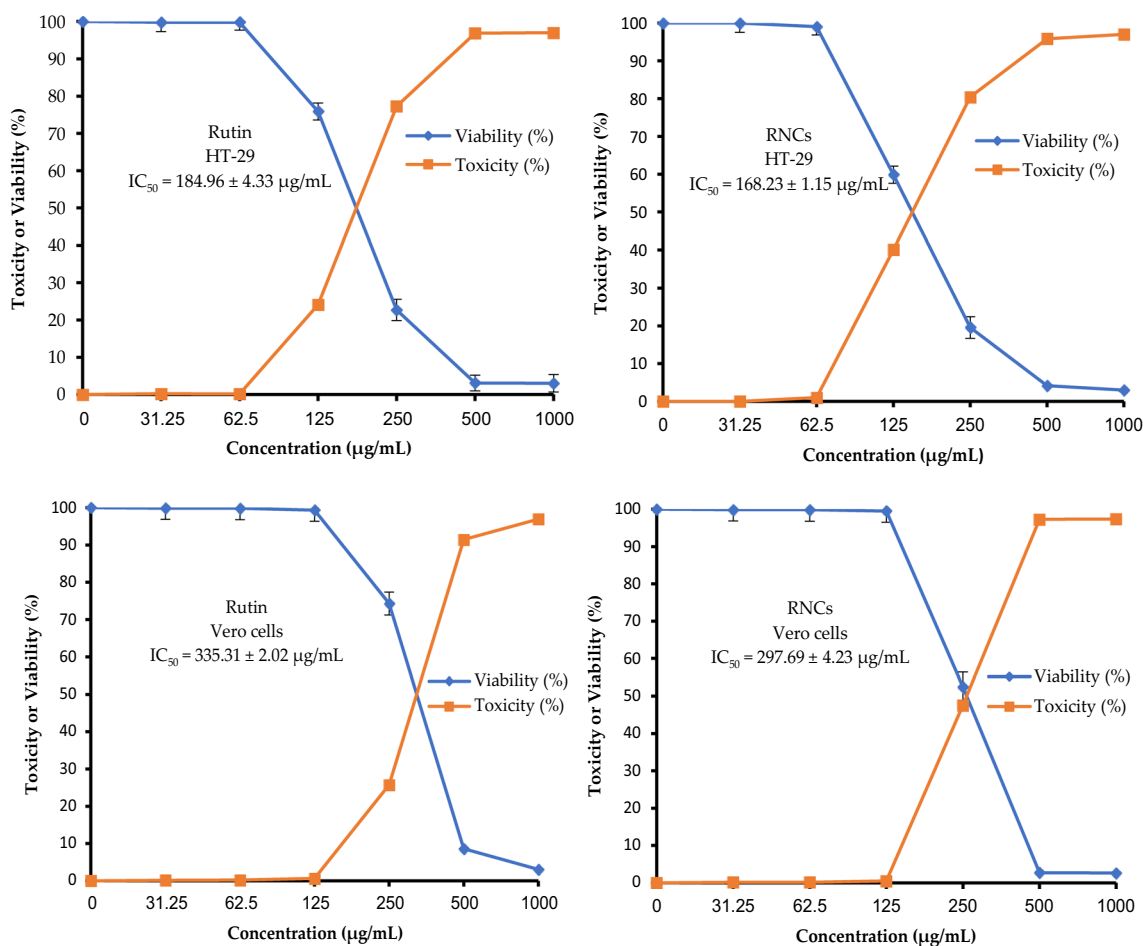


Fig. 6 Cytotoxicity of rutin and RNCs against HT-29 cell lines and normal vero cells up to 1000 µg/mL

and 1000 µg/mL including reduced confluence with lacking their well-defined morphology and presence of several dead cells (Additional file 2). The same pattern was observed in case RNCs, but more dramatic changes were recorded particularly at high concentrations 500 and 1000 µg/mL where the cells seemed rounded-shaped, as dead, separated cells with loss of polygonal form (Additional file 3). The observed changes in the morphology of HT-29 cells explained the cytotoxic influence of rutin and RNCs. Up to 250 µg/mL, Vero normal cells were not affected by rutin (Additional file 4) or RNCs (Additional file 5) but showed morphological alterations at 500 and 1000 µg/mL including apoptotic cells with cell shrinkage. All these observations were compared to the polygonal-shaped of control cells (Additional file 6) that were not exposed to rutin or RNCs. In a recent study, rutin exhibited morphological alterations in cancer cells of the colon (HCT-116) [38].

Red blood cells (RBCs) play a crucial function in delivering oxygen from the lungs to the tissues so that all cells

may get it. RBCs are continually exposed to reactive oxygen species (ROS) from both endo- and exo-genous sources throughout circulation, which damage the RBC and impair their function. Erythrocyte rupture brought on by hemolysis is a blatant sign of the harm done by these radicals and can be avoided by taking antioxidants [39]. Attractive findings were recorded for hemolysis inhibition using rutin and RNCs (Fig. 7). Different levels of hemolysis inhibition depending on the concentration of rutin or RNCs ranging from 100 to 1000 µg/mL were visualized. From the Fig. 7, RNCs exhibited more % of hemolysis inhibition (72.2, 77.3, 81.9, 87.8, 93.9 and 99.9 %) compared to hemolysis inhibition using rutin (63.6, 68.9, 73.6, 80.6, 89.8 and 97.1%) at all tested concentrations 100, 200, 400, 600, 800, and 1000 µg/mL, respectively. From the activity of indomethacin as a control drug, it's clear that RNCs are considered promising anti-hemolytic agents. It's also from the hemolysis test, RNCs do not liberate hemoglobin from RBCs. Our results were consistent with other findings [40], they showed that

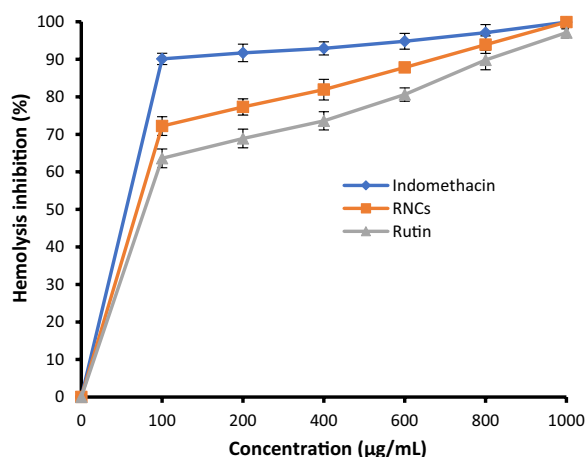


Fig. 7 Hemolysis inhibition at different concentrations of rutin and RNCs up to 1000 µg/mL compared to indomethacin as standard drug

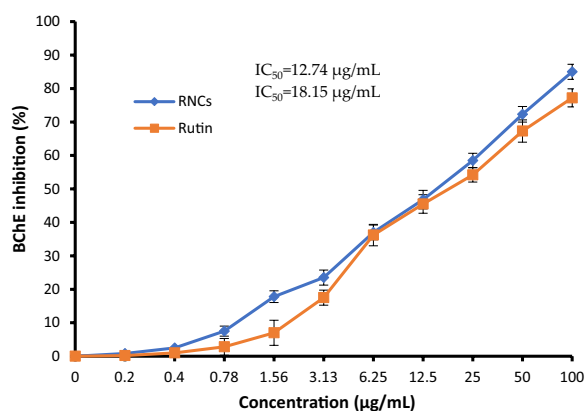


Fig. 8 Butyrylcholinesterase (BChE) inhibition at different concentrations of rutin and RNCs with IC₅₀ values

rutin provides hemolysis inhibition (69.8%) at 500 µg/mL. Rutin’s antioxidant properties help to shield the body from the cell damage caused by free radicals. It helps to improve blood flow, increase artery wall elasticity, and remove cholesterol from the body.

Butyrylcholinesterase inhibition by rutin and RNCs

In the human brain, butyrylcholinesterase (BChE), which degrades butyrylcholine (BCh), is mostly expressed in glial cells and white matter. Alzheimer’s illness is associated with significantly higher BChE levels [41]. Additionally, it is known that AChE and BChE are associated with AD and function separately from one another, which may help with disease diagnosis and the creation of prospective therapeutic targets [42]. In the present investigation, BChE inhibition % was stimulated by increasing the concentration of rutin as well as RNCs (Fig. 8), but a high level of inhibition was obtained using RNCs compared to rutin. At a concentration of 1.56 µg/mL, RNCs reflected 17.8% while rutin reflected 7% of BChE inhibition. Also, less value of RNCs IC₅₀ (12.74 µg/mL) than IC₅₀ (18.15 µg/mL) of rutin was recorded. According to Pan et al. [43], the development of Alzheimer’s disease was repressed by rutin administration. Finally, although few reports about RNCs compared to other compounds, most of the performed studies indicated that NCs exhibit the advantages of increased release of active compounds. NCs can enhance drug invasion, favour controlled release, and promote targeting, also promising littler or more attenuated side effects than traditional preparations [44]. The in vitro release of NCs formulated in pellets for pharmaceutical utilize was 3–4 times better than that of coarse particles [6].

Docking studies of rutin

Molecular docking is an appealing approach for examining chemical and protein interactions for the design and development of novel medications. The binding modes of compound can bind in different modes to a specific binding site of the protein. This is especially evident in the crystallographic structures of ligand-protein complexes. Docking of rutin was carried out with *H. pylori* (PDB code: 4HI0)₂, HT-29 (PDB code: 2HQ6), and Butyrylcholinesterase (PDB code: 6EMI) demonstrates strong behavior within the active pocket and was found a low binding score of – 7.47778 Kcal/mol, – 7.68511 Kcal/mol, and – 9.50333 Kcal/mol, respectively. The interactions in 3D are displayed in Additional files 7, 8, 9 and the

Table 2 Docking scores and energies of rutin with crystal structure of *H. pylori* 4HI0

Mol	S	rmsd_refine	E_conf	E_place	E_score1	E_refine	E_score2
Rutin	– 7.47778	1.957023	177.1588	– 62.5887	– 10.5208	– 27.7999	– 7.47778
Rutin	– 7.30962	1.51214	140.1248	– 74.3798	– 10.9772	– 44.6774	– 7.30962
Rutin	– 6.94588	1.932674	133.3282	– 86.3139	– 12.1694	– 41.521	– 6.94588
Rutin	– 6.7668	3.867486	131.0068	– 90.865	– 10.8535	– 39.5178	– 6.7668
Rutin	– 6.71519	2.079944	132.2194	– 87.5385	– 10.3369	– 30.4621	– 6.71519

Table 3 Docking scores and energies of rutin with crystal structures of colon cancer 2HQ6 and butyrylcholinesterase 6EMI

Mol	Colon cancer 2HQ6						
	S	rmsd_refine	E_conf	E_place	E_score1	E_refine	E_score2
Rutin	-7.68511	2.349049	132.271	-123.92	-13.0537	-49.3727	-7.68511
Rutin	-7.60016	2.348212	126.5045	-103.569	-12.23	-44.203	-7.60016
Rutin	-7.39895	1.889362	129.7233	-150.22	-14.7096	-48.5907	-7.39895
Rutin	-7.3079	1.897974	129.4777	-110.06	-12.5711	-45.2671	-7.3079
Rutin	-6.99121	1.554326	138.5355	-87.1548	-12.5681	-40.8826	-6.99121
Butyrylcholinesterase 6EMI							
Rutin	-9.50333	1.890657	152.8203	-75.8811	-13.4338	-53.1697	-9.50333
Rutin	-9.29916	2.056552	130.7517	-118.942	-14.2454	-51.3429	-9.29916
Rutin	-9.04007	3.989687	278.5143	-73.1489	-14.115	-54.701	-9.04007
Rutin	-8.99539	2.91718	147.4303	-120.081	-14.2492	-58.3387	-8.99539
Rutin	-8.81397	2.213047	134.2875	-71.2674	-15.1458	-46.3784	-8.81397

Table 4 Interaction of rutin with crystal structure of *H. pylori* 4HI0

Mol	Ligand	Receptor	Interaction	Distance	E (kcal/mol)
Rutin	O 13	O PRO 111 (B)	H-donor	2.62	-2.6
	O 47	OE1 GLU 251 (B)	H-donor	2.67	-2.0
	O 64	OE1 GLU 251 (B)	H-donor	2.70	-2.9
	O 66	OE2 GLU 47 (B)	H-donor	3.04	-2.6
	O 47	NH1 ARG 250 (B)	H-acceptor	2.74	-2.7
	O 64	NH1 ARG 76 (B)	H-acceptor	3.16	-1.5
	6-ring	CA GLN 80 (B)	Pi-H	3.96	-0.7

binding energies are given in Tables 2, 3. Rutin formed seven interaction bonds against 4HI0 protein by amino acid residues (PRO 111, GLU 251, GLU 47, ARG 250, ARG 76, GLN 80) through (O13, O 47, O 64, O 66, O47,

O 64, 6-ring) respectively as recommended in table 4. While in the case of 2HQ6 protein (HT-29) showed four hydrogen bonding between oxygen atoms (O 11, O 13, O 68, and O 45) of rutin towards ASP 108, GLY 74, ASP 152, and GLN 64 amino acid residues (Table 5). The hydrogen bond varied from 2.99 to 3.30 Å distance and the energy stabilization by -1.0 to -2.2 K cal. Also, it was found that rutin exhibited the best docking score according to its interaction with 6EMI protein (Butyrylcholinesterase) through O 11, O 28, O 64, and C 70 atoms with GLU 197, SER 287, ASP 70, and TRP 430 amino acid residues as hydrogen bonding interactions with the key amino acid residues of the identified binding pockets based on the output in Table 5, stabilized the structure of the target receptor. The MOE-Dock examination is trustworthy for docking this inhibitor, and the RMSD values were found to be 1.957, 2.349, and 1.89 Å for 4HI0, 2HQ6, and 6EMI, respectively, proving that our docking method is suitable for the studied inhibitor. All the docked pose with the least binding energy has the

Table 5 Interaction of rutin with crystal structures of colon cancer 2HQ6 and butyrylcholinesterase 6EMI

Mol	Colon cancer 2HQ6				
	Ligand	Receptor	Interaction	Distance	E (kcal/mol)
Rutin	O 11	O ASP 108 (A)	H-donor	3.30	-1.1
	O 13	O GLY 74 (A)	H-donor	3.04	-2.1
	O 68	O ASP 152 (A)	H-donor	3.17	-1.0
	O 45	NE2 GLN 64 (A)	H-acceptor	2.99	-2.2
Butyrylcholinesterase 6EMI					
Rutin	O 11	OE1 GLU 197 (A)	H-donor	3.02	-3.8
	O 28	O SER 287 (A)	H-donor	3.00	-1.3
	O 64	OD2 ASP 70 (A)	H-donor	2.91	-2.4
	C 70	5-ring TRP 430 (A)	H-Pi	4.63	-0.5

highest affinity, thereby, is considered the best docked conformation. Docking interaction of chlorogenic acid and ferulic acid with 4HI0 protein enzyme of *H. pylori* resulted in low energy scores of -6.4876 kcal/mol [14] and -5.58 Kcal/mol [20] but not the same energy score (-7.47778 Kcal/mol) in the current study. As mentioned in other reports, the high value of the negative score indicated the inhibitory potential of compounds against target cells [12, 21, 22, 45, 46], therefore negative score value of the free binding energy in the current study documents the biological efficacy of rutin. Also, a low energy score of -8.9 kcal/mol was recorded as a result of rutin docked with the main protease of severe acute respiratory syndrome coronavirus-2 [47]. In another study, a higher binding affinity was recorded using rutin among different natural flavonoids for monoamine oxidase, butyrylcholinesterase, and acetylcholinesterase with low energy scores of -12.0 , -12.2 , -12.6 , respectively [48]. The obtained findings from docking interaction revealed that rutin may be a candidate as an inhibitor for *H. pylori*, HT-29 cells and BChE. Numerous still unanswered questions remain about rutin and RNCs. In light of this, other biological investigations against various microorganisms and cancer cell lines, besides in vivo tests, will be planned to support and confirm the obtained findings. Moreover, the mechanisms for biological activities of rutin and RNCs should be the focus of additional investigations in the future.

Supplementary Information

The online version contains supplementary material available at <https://doi.org/10.1186/s13765-023-00832-z>.

Additional file 1: FTIR of rutin (A) and RNCs (B) showed more than 20 similar bands in rutin and RNCs, such as 3423.36, 1656.52, 1599.71, 1572.91, 1555.98, 1504.85, 1456.94, 1362.06, 1294.85, 1234.25, 1203.67, 1012.16, 969.85, 878.94, 806.41, 688.55, 726.17, 655.42, 630.15, 595.90, and 531.59 cm^{-1} in rutin which similar to the detected bands 3423.23, 1655.58, 1598.82, 1573.57, 1556.63, 1504.97, 1457.86, 1361.17, 1295.60, 1236.47, 1204.21, 1012.83, 970.90, 878.98, 806.51, 687.89, 725.93, 655.47, 630.60, 596.19, and 531.76 cm^{-1} in RNCs.

Additional file 2: Morphological features of HT-29 cell exposed to different concentrations of rutin including 31.25 $\mu\text{g}/\text{mL}$ (A), 62.5 $\mu\text{g}/\text{mL}$ (B), 125 $\mu\text{g}/\text{mL}$ (C), 250 $\mu\text{g}/\text{mL}$ (D), 500 $\mu\text{g}/\text{mL}$ (E) and 1000 $\mu\text{g}/\text{mL}$ (F). No seemed morphological changes at 31.25 $\mu\text{g}/\text{mL}$ and 62.5 $\mu\text{g}/\text{mL}$, while at 250 to 1000 $\mu\text{g}/\text{mL}$ notable changes were appeared such as reduced confluence with lacking well-defined morphology and occurrence of numerous dead cells.

Additional file 3: Morphological features of HT-29 cell exposed to different concentrations of RNCs. 31.25 $\mu\text{g}/\text{mL}$ (A), 62.5 $\mu\text{g}/\text{mL}$ (B), 125 $\mu\text{g}/\text{mL}$ (C), 250 $\mu\text{g}/\text{mL}$ (D), 500 $\mu\text{g}/\text{mL}$ (E) and 1000 $\mu\text{g}/\text{mL}$ (F). Visualized alteration were documented particularly at high concentrations 500 and 1000 $\mu\text{g}/\text{mL}$ where the cells seemed rounded-shaped, as dead, separated cells with loss of polygonal form

Additional file 4: Morphological features of Vero cell exposed to different concentrations of rutin. 31.25 $\mu\text{g}/\text{mL}$ (A), 62.5 $\mu\text{g}/\text{mL}$ (B), 125 $\mu\text{g}/\text{mL}$ (C), 250 $\mu\text{g}/\text{mL}$ (D), 500 $\mu\text{g}/\text{mL}$ (E) and 1000 $\mu\text{g}/\text{mL}$ (F). Vero normal cells were not affected by rutin up to 250 $\mu\text{g}/\text{mL}$ but morphological changes

was observed at 500 and 1000 $\mu\text{g}/\text{mL}$ including apoptotic cells with cell shrinkage.

Additional file 5: Morphological features of Vero cell exposed to different concentrations of RNCs. 31.25 $\mu\text{g}/\text{mL}$ (A), 62.5 $\mu\text{g}/\text{mL}$ (B), 125 $\mu\text{g}/\text{mL}$ (C), 250 $\mu\text{g}/\text{mL}$ (D), 500 $\mu\text{g}/\text{mL}$ (E) and 1000 $\mu\text{g}/\text{mL}$ (F). Up to 250 $\mu\text{g}/\text{mL}$, Vero normal cells were not affected by RNCs up to 250 $\mu\text{g}/\text{mL}$ but morphological changes was observed at 500 and 1000 $\mu\text{g}/\text{mL}$ including apoptotic cells with cell shrinkage as in case rutin.

Additional file 6: Polygonal-shaped of control cells of HT-29 cells (A) and Vero cells (Unexposed to rutin or RNCs) (B).

Additional file 7: Molecular docking process of rutin with 4HI0. A The interaction between rutin and active sites of 4HI0 protein; B the most likely binding conformation of rutin and the corresponding intermolecular interactions are identified; C molecular surface of rutin with 4HI0; D the contact preference of rutin with 4HI0; E interaction potential of rutin with 4HI0; F the Electrostatic map of rutin with 4HI0.

Additional file 8: Molecular docking process of rutin with 2HQ6; A the interaction between rutin and active sites of 2HQ6 protein; B the most likely binding conformation of rutin and the corresponding intermolecular interactions are identified; C molecular surface of rutin with 2HQ6; D the contact preference of rutin with 2HQ6; E interaction potential of rutin with 2HQ6; F the Electrostatic map of rutin with 2HQ6.

Additional file 9: Molecular docking process of rutin with 6EMI. A The interaction between rutin and active sites of 6EMI protein; B the most likely binding conformation of rutin and the corresponding intermolecular interactions are identified; C molecular surface of rutin with 6EMI; D the contact preference of rutin with 6EMI; E interaction potential of rutin with 6EMI; F the Electrostatic map of rutin with 6EMI.

Acknowledgements

To Princess Nourah bint Abdulrahman University Researchers Supporting Project number (PNURSP2023R217), Princess Nourah bint Abdulrahman University, Riyadh, Saudi Arabia. To Dr. Yahya Ali for English editing.

Author contributions

HQ and AMHA Carried out some of the experiments, review and editing, MNA; carried out some experiments and writing—original draft preparation, AAB; investigation and formal analysis, MSH and TMA; carried out the experiment of antimicrobial activities, formal analysis and edited the manuscript, MNA and MSH; designed some experiments and wrote the paper, TMA; wrote the paper, review and editing. All authors have read and agreed to the published version of the manuscript.

Funding

This research was funded by Princess Nourah bint Abdulrahman University Researchers Supporting Project number (PNURSP2023R217), Princess Nourah bint Abdulrahman University, Riyadh, Saudi Arabia.

Availability of data and materials

All data that support the findings of this study are available within the article.

Declarations

Competing interests

All authors declare no competing interests.

Author details

¹Department of Medical Laboratory Science, College of Applied Medical Sciences, University of Ha'il, 55476 Hail, Saudi Arabia. ²Department of Biology, College of Science, Princess Nourah bint Abdulrahman University, P.O. Box 84428, Riyadh 11671, Saudi Arabia. ³Department of Medical Laboratory Sciences, Faculty of Applied Medical Sciences, King Abdulaziz University, 22254 Jeddah, Saudi Arabia. ⁴Hematology Research Unit, King Fahd Medical Research Center, King Abdulaziz University, 22254 Jeddah, Saudi Arabia. ⁵Botany and Microbiology Department, Faculty of Science, Al-Azhar University, Nasr City, Cairo 11725, Egypt. ⁶Medical and Diagnostic Research Center, University of Ha'il, Hail 55473, Saudi Arabia.

Received: 28 June 2023 Accepted: 25 September 2023

Published online: 17 November 2023

References

- Mauludin R, Müller RH, Keck CM (2009) Development of an oral rutin nanocrystal formulation. *Int J Pharm* 370:202–209
- Imani A, Maleki N, Bohlouli S, Kouhsoltani M, Sharifi S, Dizaj SM (2020) Molecular mechanisms of anticancer effect of rutin. *Phytother Res* 35:2500–2513
- Negahdari R, Bohlouli S, Sharifi S, Dizaj SM, Saadat YR, Khezri K, Jafari S, Ahmadian E, Jahandizi NG, Raeesi S (2021) Therapeutic benefits of rutin and its nanoformulations. *Phytother Res* 35:1719–1738
- Memar MY, Yekani M, Sharifi S, Dizaj SM (2022) Antibacterial and biofilm inhibitory effects of rutin nanocrystals. *Biointerface Res Appl Chem* 13:132
- Hassan AS, Soliman GM (2022) Rutin nanocrystals with enhanced anti-inflammatory activity: preparation and ex vivo/in vivo evaluation in an inflammatory rat model. *Pharmaceutics* 14(12):2727. <https://doi.org/10.3390/pharmaceutics14122727>
- Wang Y-D, Zhang Y, Sun B, Leng X-W, Li Y-J, Ren L-Q (2018) Cardioprotective effects of rutin in rats exposed to pirarubicin toxicity. *J Asian Nat Prod Res* 20:361–373
- Oyagbemi AA, Bolaji-Alabi FB, Ajibade TO, Adejumo OA, Ajani OS, Jarikre TA, Omobowale TO, Ola-Davies OE, Soetan KO, Aro AO et al (2020) Novel antihypertensive action of rutin is mediated via inhibition of angiotensin converting enzyme/mineralocorticoid receptor/angiotensin 2 type 1 receptor (ATR1) signaling pathways in uninephrectomized hypertensive rats. *J Food Biochem* 44:e13534
- Orhan DD, Özçelik B, Özgen S, Ergun F (2010) Antibacterial, antifungal, and antiviral activities of some flavonoids. *Microbiol Res* 165:496–504. <https://doi.org/10.1016/j.micres.2009.09.002>
- Gullón B, Lu-Chau TA, Moreira MT, Lema JM, Eibes G (2017) Rutin: a review on extraction, identification and purification methods, biological activities and approaches to enhance its bioavailability. *Trends Food Sci Technol* 67:220–235
- Pelikh O, Stahr P-L, Huang J, Gerst M, Scholz P, Dietrich H, Geisel N, Keck CM (2018) Nanocrystals for improved dermal drug delivery. *Eur J Pharm Biopharm* 128:170–178
- Wu H, Su M, Jin H, Li X, Wang P, Chen J, Chen J (2020) Rutin-loaded silver nanoparticles with antithrombotic function. *Front Bioeng Biotechnol* 8:598977
- Al-Rajhi AMH, Yahya R, Abdelghany TM, Fareid MA, Mohamed AM, Amin BH, Masrahi AS (2022) Anticancer, anticoagulant, antioxidant and antimicrobial activities of *Thevetia peruviana* latex with molecular docking of antimicrobial and anticancer activities. *Molecules* 27:3165. <https://doi.org/10.3390/molecules27103165>
- Qanash H, Bazaid AS, Binsaleh NK, Alharbi B, Alshammari N, Qahl SH, Alhuthali HM, Bagher AA (2023) Phytochemical characterization of Saudi mint and its mediating effect on the production of silver nanoparticles and its antimicrobial and antioxidant activities. *Plants* 12:2177
- Yahya R, Al-Rajhi AMH, Alzaid SZ, Al Abboud MA, Almuhayawi MS, Al Jaouni SK, Selim S, Ismail KS, Abdelghany TM (2022) Molecular docking and efficacy of *Aloe vera* gel based on chitosan nanoparticles against *Helicobacter pylori* and its antioxidant and anti-inflammatory activities. *Polymers* 14(15):2994. <https://doi.org/10.3390/polym14152994>
- Xu PX, Wang SW, Yu XL, Su YJ, Wang T, Zhou WW, Liu RT (2014) Rutin improves spatial memory in Alzheimer's disease transgenic mice by reducing A β oligomer level and attenuating oxidative stress and neuroinflammation. *Behav Brain Res* 264:173–180. <https://doi.org/10.1016/j.bbr.2014.02.002>
- Habtemariam S (2016) Rutin as a natural therapy for Alzheimer's disease: insights into its mechanisms of action. *Curr Med Chem* 23(9):860–873. <https://doi.org/10.2174/09298673233666160217124333>
- Patel K, Patel DK (2019) The beneficial role of rutin, a naturally occurring flavonoid in health promotion and disease prevention: a systematic review and update. In: Preedy VR, Watson RR (eds) *Bioactive food as dietary interventions for arthritis and related inflammatory diseases*, 2nd edn. Academic Press, Cambridge, pp 457–479
- Satari A, Ghasemi S, Habtemariam S, Asgharian S, Lorigooini Z (2021) Rutin: a flavonoid as an effective sensitizer for anticancer therapy; insights into multifaceted mechanisms and applicability for combination therapy. *Evid Based Complement Alternat Med* 23(2021):9913179. <https://doi.org/10.1155/2021/9913179>
- Alawlaqi MM, Al-Rajhi AMH, Abdelghany TM, Ganash M, Moawad H (2023) Evaluation of biomedical applications for linseed extract: antimicrobial, antioxidant, anti-diabetic, and anti-inflammatory activities in vitro. *J Funct Biomater* 14(6):300. <https://doi.org/10.3390/jfb14060300>
- Al-Rajhi AMH, Qanash H, Bazaid AS, Binsaleh NK, Abdelghany TM (2023) Pharmacological evaluation of *Acacia nilotica* flower extract against *Helicobacter pylori* and human hepatocellular carcinoma in vitro and in silico. *J Funct Biomater* 14(4):237. <https://doi.org/10.3390/jfb14040237>
- Al-Rajhi AM, Abdelghany TM (2023) Nanoemulsions of some edible oils and their antimicrobial, antioxidant, and anti-hemolytic activities. *BioResources* 18(1):1465–1481. <https://doi.org/10.15376/biores.18.1.1465-1481>
- Al-Rajhi AMH, Abdelghany TM (2023) In vitro repress of breast cancer by bio-product of edible *Pleurotus ostreatus* loaded with chitosan nanoparticles. *Appl Biol Chem* 66:33. <https://doi.org/10.1186/s13765-023-00788-0>
- Sabbagh GM, Al-Beik LM, Hadid I (2023) In silico and in vitro anticoagulant activity detection of quercetin, rutin, and troxerutin as new potential inhibitors of factor Xa. *Egypt J Chem* 66(2):151–166. <https://doi.org/10.21608/ejchem.2022.140123.6144>
- Castillo-Juarez I, Rivero-Cruz F, Celis H, Romero I (2007) Anti-*Helicobacter pylori* activity of anacardic acids from *Amphipterygium adstringens*. *J Ethnopharmacol* 114(1):72–77
- French GL (2006) Bactericidal agents in the treatment of MRSA infections—the potential role of daptomycin. *J Antimicrob Chemother* 58:1107
- Antunes ALS, Trentin DS, Bonfanti JW, Pinto CCF, Perez LRR, Macedo AJ, Barth AL (2010) Application of a feasible method for determination of biofilm antimicrobial susceptibility in staphylococci. *APMIS* 118:873–877. <https://doi.org/10.1111/j.1600-0463.2010.02681.x>
- Mahernia S, Bagherzadeh K, Mojab F, Amanlou M (2015) Urease inhibitory activities of some commonly consumed herbal medicines. *Iran J Pharm Res* 14(3):943–947
- Pistia-Brueggeman G, Hollingsworth RI (2001) A preparation and screening strategy for glycosidase inhibitors. *Tetrahedron* 57(42):8773–8778
- Ellman GL, Courtney KD, Andres V Jr, Feather-Stone RM (1961) A new and rapid colorimetric determination of acetylcholinesterase activity. *Biochem Pharmacol* 7:88–95
- Bohlouli S, Jafarmadar Gharehbagh F, Dalir Abdolahinia E, Kouhsoltani M, Ebrahimi G, Roshangar L, Imani A, Sharifi S, Dizaj MS (2021) Preparation, characterization, and evaluation of rutin nanocrystals as an anticancer agent against head and neck squamous cell carcinoma cell line. *J Nanomater*. <https://doi.org/10.1155/2021/9980451>
- Jeong C-S (2009) Evaluation for protective effect of rutin, a natural flavonoid, against HCl/ethanol-induced gastric lesions. *Biomol Ther* 17:199–204. <https://doi.org/10.4062/biomolther.2009.17.2.199>
- Samiei M, Farjami A, Maleki Dizaj S, Lotfipour F (2016) Nanoparticles for antimicrobial purposes in endodontics: a systematic review of in vitro studies. *Mater Sci Eng, C* 58:1269–1278. <https://doi.org/10.1016/j.msec.2015.08.070>
- Al-Shabib NA, Husain FM, Ahmad I, Khan MS, Khan RA, Khan JM (2017) Rutin inhibits mono and multi-species biofilm formation by foodborne drug resistant *Escherichia coli* and *Staphylococcus aureus*. *Food Control* 79:325–332. <https://doi.org/10.1016/j.foodcont.2017.03.004>
- Wang Z, Ding Z, Li Z, Ding Y, Jiang F, Liu J (2021) Antioxidant and antibacterial study of 10 flavonoids revealed rutin as a potential antibiofilm agent in *Klebsiella pneumoniae* strains isolated from hospitalized patients. *Microb Pathog* 159:105121
- Ahmad M, Sahabjada JA, Hussain A, Badaruddeen MA, Mishra A (2017) Development of a new rutin nanoemulsion and its application on prostate carcinoma PC3 cell line. *EXCLI J* 16:810
- Asfour MH, Mohsen AM (2018) Formulation and evaluation of pH-sensitive rutin nanospheres against colon carcinoma using HCT-116 cell line. *J Adv Res* 9:17–26
- Guon TE, Chung HS (2016) Hyperoside and rutin of *Nelumbo nucifera* induce mitochondrial apoptosis through a caspase-dependent mechanism in HT-29 human colon cancer cells. *Oncol Lett* 11(4):2463–2470

38. Ismail A, El-Biyally E, Sakran W (2023) An innovative approach for formulation of rutin tablets targeted for colon cancer treatment. *AAPS PharmSciTech* 24(2):68. <https://doi.org/10.1208/s12249-023-02518-7>
39. Thakur P, Chawla R, Narula A, Goel R, Arora R, Sharma RK (2016) Anti-hemolytic, hemagglutination inhibition and bacterial membrane disruptive properties of selected herbal extracts attenuate virulence of Carbapenem Resistant *Escherichia coli*. *Microb Pathog* 95:133–141. <https://doi.org/10.1016/j.micpath.2016.04.005>
40. Ramani S, Basak S, Puneeth S, Mahato K, Malathi R (2021) Anti hemolytic activity of rutin in case of phenyl hydrazine induced hemolysis. *Curr Trends in BiotechnolPharm* 15(5):467–470. <https://doi.org/10.5530/ctbp.2021.3s.41>
41. Kumar A, Pintus F, Di Petrillo A, Medda R, Caria P, Matos MJ, Fais A (2018) Novel 2-phenylbenzofuran derivatives as selective butyrylcholinesterase inhibitors for Alzheimer's disease. *Sci Rep* 8(1):4424
42. Lake F (2013) BChE reported to be associated with plaque level in Alzheimer's disease. *Biomark Med* 7:197–198
43. Pan RY, Ma J, Kong XX, Wang XF, Li SS, Qi XL, Yuan Z (2019) Sodium rutin ameliorates Alzheimer's disease-like pathology by enhancing microglial amyloid- β clearance. *Sci Adv* 5(2):eaau6328. <https://doi.org/10.1126/sciadv.aau6328>
44. Su Y, Gao J, Dong X, Wheeler KA, Wang Z. Neutrophil-Mediated Delivery of Nanocrystal Drugs via Photoinduced Inflammation Enhances Cancer Therapy. *ACS Nano*. 2023 Aug 22;17(16):15542-15555. <https://doi.org/10.1021/acsnano.3c02013>.
45. Qanash H, Bazaid AS, Aldarhami A, Alharbi B, Almashjary MN, Hazzazi MS, Felemban HR, Abdelghany TM (2023) Phytochemical characterization and efficacy of *Artemisia judaica* extract loaded chitosan nanoparticles as inhibitors of cancer proliferation and microbial growth. *Polymers* 15(2):391. <https://doi.org/10.3390/polym15020391>
46. Qanash H, Yahya R, Bakri MM, Bazaid AS, Qanash S, Shater AF, Abdelghany TM (2022) Anticancer, antioxidant, antiviral and antimicrobial activities of Kei Apple (*Dovyalis caffra*) fruit. *Sci Rep* 12:5914. <https://doi.org/10.1038/s41598-022-09993-1>
47. Rahman F, Tabrez S, Ali R, Alqahtani AS, Ahmed MZ, Rub A (2021) Molecular docking analysis of rutin reveals possible inhibition of SARS-CoV-2 vital proteins. *J Tradit Complement Med* 11(2):173–179. <https://doi.org/10.1016/j.jtcme.2021.01.006>
48. Ishola AA, Oyinloye BE, Ajiboye BO, Kappo AP (2021) Molecular docking studies of flavonoids from *Andrographis paniculata* as potential acetylcholinesterase, butyrylcholinesterase and monoamine oxidase inhibitors towards the treatment of neurodegenerative diseases. *Biointerface Res Appl Chem* 11:9871–9879

Publisher's Note

Springer Nature remains neutral with regard to jurisdictional claims in published maps and institutional affiliations.

Submit your manuscript to a SpringerOpen[®] journal and benefit from:

- Convenient online submission
- Rigorous peer review
- Open access: articles freely available online
- High visibility within the field
- Retaining the copyright to your article

Submit your next manuscript at ► [springeropen.com](https://www.springeropen.com)
